Journal of Alloys and Compounds 680 (2016) 232–236

Contents lists available at ScienceDirect

Journal of Alloys and Compounds

journal homepage: http://www.elsevier.com/locate/jalcom

Enhanced resonant Raman scattering and optical emission of ZnO/ZnMgO multiple quantum wells

Q.Y. Zhang*, J.M. Ashfaq, B.C. Hu, J.Y. Wang, N. Zhou

Key Laboratory of Materials Modification by Laser, Ion and Electron Beams, School of Physics and Opto-electronic Technology, Dalian University of Technology, Dalian 116024, China

ARTICLE INFO

Article history:
Received 18 March 2016
Received in revised form
13 April 2016
Accepted 16 April 2016
Available online 19 April 2016

Keywords:
ZnO/ZnMgO
MQWs
Quantum-confinement effect
Resonant Raman scattering

ABSTRACT

Multiple quantum wells (MQWs) with well-defined multilayer structure are at the foundation of fabricating optoelectronic devices with high quantum efficiency. In this study, we report the ZnO/ZnMgO MQWs fabricated under optimized conditions. At room temperature, the MQW samples, excited by a 325-nm He-Cd laser, exhibited intense ultraviolet photoluminescence (PL) tuned by the quantum confinement (QC) effect. At the same time, extremely enhanced multiple-phonon resonant Raman scattering (RRS) was observed in the first time in the PL spectra of ZnO-based MQW samples. The multiple-phonon RRS was ascribed to the ingoing and outgoing resonance with the barrier layers, and was found highly in accordance with that of ZnMgO epilayer deposited under the same conditions, thus strongly evidencing the MQW samples have well-defined multilayer structures. Using the PL spectra taken at ~12 K, the PL shifts induced by QC effect were found in good agreement with the calculated results using Kronig-Penney model.

1. Introduction

Since the reports on the stimulated emission at room temperature (RT) [1–3], ZnO has received much attention in the past decades. As an important wide-gap oxide semiconductor, ZnO has a band gap of ~3.3 eV, thus is considered as a potential candidate in applications of ultraviolet (UV) opto-electronic devices, such as light-emitting diode, laser diode, and UV detector. Optically pumped ZnO films have been demonstrated RT laser action with a low threshold (24 kW/cm^2) [1–3], due to its high exciton binding energy (60 meV) [4]. On the other hand, $Zn_{1-x}Mg_xO$ alloy with the lattice constants similar to ZnO shows a higher band gap, up to 4 eV at $x = 0.33$ [5], thus low-dimensional ZnO/ZnMgO structures forming quantum wells are expected to further enhance the optical emission process with exciton recombination. As a matter of fact, Ohtomo et al. have reported the optimized multiple quantum wells (MQWs) having the threshold of the stimulated emission as low as 11 kW/cm^2 [6], far better than ZnO epilayers.

To further improve the ZnO/ZnMgO MQWs, growth of MQW samples was explored using the methods such as pulsed laser deposition (PLD), molecular beam epitaxy (MBE), and magnetron sputtering, as well as using various substrates including sapphire, $ScMgAlO_4$, ZnO, and Si [7–15], among which sapphire is preferred. Though the reported optical emissions of these MQW samples are quite different, it is commonly accepted that *c*-axis sapphire facilitates the growth of MQW samples with low density of structure defects, but piezoelectric and spontaneous polarization effects are frequently present in the biaxially strained wurtzite epilayers with the *c*-axis parallel to the growth direction. Therefore, the quantum efficiency of photoluminescence (PL) is considerably reduced, because the electron-hole pairs are spatially separated due to the quantum-confined Stark (QCS) and Franz-Keldysh (QCFK) effects [16–18]. Makino et al. [16] found that QCS and QCFK effects cannot be observed unless both of the following conditions are accomplished: (1) higher Mg concentration ($x \geq 0.27$) and (2) the thickness of well layer $L_w \geq 4.23$ nm. Therefore, the MQW samples are better fabricated using the ZnMgO barrier layer with a relatively low Mg content. At the same time, the well layer should be thin enough ($L_w \leq 4$ nm). In fact, the MQW samples with $L_w \geq 4$ nm cannot provide sufficiently large PL shifts, thus are not important in fabrication of MQW-based optoelectronic devices. In addition, Brandt et al. [19] showed that the QCS effect could be reduced using sufficient high energy-fluence during deposition of MQW samples by PLD method.

* Corresponding author.
E-mail address: qyzhang@dlut.edu.cn (Q.Y. Zhang).

http://dx.doi.org/10.1016/j.jallcom.2016.04.150
0925-8388/

In this work, ZnO/ZnMgO MQW samples were fabricated using PLD method under optimized conditions effectively avoiding the QCS effects. Excited by a 325-nm He-Cd laser, the MQW samples emitted intensive UV light obviously tuned by quantum confinement (QC) effect. The PL spectra were studied by changing the temperature from RT down to ~12 K, and the PL shift induced by QC effect was quantitatively in good agreement with the results calculated using Kronig-Penney model. Furthermore, an enhanced multiple-phonon resonant Raman scattering (RRS) was observed in the first time in the ZnO/ZnMgO MQW samples, and was further demonstrated originating from the enhancement in Raman scattering caused by the ingoing and outgoing resonance with the barrier layers.

2. Experimental details

The ZnO/ZnMgO MQWs were grown on epi-polished (0001) sapphire substrate at optimized parameters of 800 °C and ~1×10^{-4} Pa by alternatively depositing ZnO and ZnMgO layers. ZnO (99.99% purity) and $Zn_{0.9}Mg_{0.1}O$ ceramic targets were used for growth of the well and the barrier layers, respectively. Prior to the deposition of MQW layers, a ~20-nm-thick ZnO buffer layer was deposited at 800 °C and ~1×10^{-4} Pa, and then the MQWs with ten periods were fabricated on the ZnO buffer layer. Deposition time was used to control the layer thickness by predetermining the growth rate in the single-layer deposition experiments. The deposition of ZnO and ZnMgO layers were optimized at a growth rate of ~1.0 nm/min by fitting the transmittance spectra of the single layer samples. The ZnO well layers were varied from 1.4 to 3.0 nm in thickness, maintaining the barrier layer constant at ~7 nm. Further details on growth of MQWs can be found in our previous publication [20].

The ZnO and ZnMgO single-layer films as well as the MQW samples were characterized by x-ray diffraction (XRD) using Bruker-D_8 diffractometer in terms of coupled scan, rocking curve, ϕ-scan, reciprocal space map (RSM), and x-ray reflectance (XRR). The surface morphology of the film samples was examined by scanning electron microscopy (SEM, Hitachi S-4800) and contact-mode atomic force microscopy ΣAFM, Benyuan SPM5000Π> PL spectra were collected using FLS 920 fluorescence spectrometer with an L-shape path and varying the temperature from RT to ~12 K. A ~3 W/cm^2 He-Cd laser operating at wavelength of 325 nm was used for PL excitation.

3. Results and discussion

Before fabrication of MQW samples, the growth of ZnO and ZnMgO single-layer films was first optimized. Temperature and pressure were found to be the two important factors influencing the film roughness, which is rather crucial to control the formation of MQWs with sharp interfaces. SEM images showed that ~120-nm-thick ZnO and ZnMgO films deposited at ~1×10^{-4} Pa and 800 °C have smooth morphology in a large scale, as shown in Fig. 1(a) and (b). No grain boundary could be found in the SEM images as well as in 2 μm × 2 μm AFM images, indicating the as-grown ZnO and ZnMgO films are single-crystalline. The rms roughness was determined to be 0.55 and 1.25 nm for the ZnO and ZnMgO films, respectively. These values are not good enough, but still are the better roughness for a 120-nm thick ZnO or ZnMgO layer obtained using PLD method and sufficiently smooth for fabrication of MQW samples. XRD analysis revealed the highly epitaxial ZnO and ZnMgO films having good crystallinity. The full width at half maximum (FWHM) of the (0002) XRD ω-rocking curves was determined to be ~0.032° (~115 arc sec) and ~0.25° (900 arc sec) for the ZnO and ZnMgO epilayers, respectively, as shown in the insets of Fig. 1. In comparison with the reports on the samples prepared by PLD methods, this FWHM value is rather small for ZnO epilayers grown on sapphire, but still larger than that on the lattice-matched $ScAlMgO_4$ substrate (12 arc sec) [21].

The MQW samples with the multilayer structure, as schematically depicted in the inset of Fig. 2, were fabricated at the optimized conditions, and were further evidenced by XRR. XRD revealed that the MQWs have the FWHMs of (0002) ω-rocking curves a little larger than that of the single epilayers, slowly increases from 0.27° to 0.34° with the increase in the well-layer thickness when $L_w \leq 2.3$ nm, and abruptly changes to be larger than 0.55° when $L_w \geq 2.6$ nm. The symmetric RSMs of (0002) diffraction showed that the deviation between the ZnO and ZnMgO layers is hardly observed in the MQW samples with $L_w \leq 2.3$ nm, but is visible when $L_w \geq 2.6$ nm, as shown in the supporting materials (Fig. S1), suggesting that the crystallinity of MQW samples with $L_w \leq 2.3$ nm is good enough, but goes worse when $L_w \geq 2.6$ nm. Excited by the He-Cd laser operating at 325 nm, all the MQW samples emitted intense UV light at RT. With the decrease in the thickness of well layers, the QC effect produced a systematic blue-shift with respect to the PL peak of ZnO epilayer, as shown in Fig. 2, in which the PL spectra of ZnO and ZnMgO epilayers were included for comparison. The PL from the buffer layers is almost invisible at RT, indicative of the high PL efficiency of the MQW samples.

Differing from previous reports, there are as many as four sharp peaks appearing in the PL spectra at the high-energy side with respect to the PL peaks of MQWs. These sharp-peak structures have equal intervals independent of the variation in the thickness of well layers, thus we assigned them to multiple-phonon RRS. RRS by the longitudinal optical (LO) phonons is usually observed in polar semiconductors, when the sample is excited by the light with photon energy larger than the band gap. However, multiple-phonon RRS has never been reported in ZnO-based MQWs, probably due to the alloying effect of the barrier and well layers, though multilayer structures in these MQW samples were usually evidenced by XRR. The Raman peaks in our MQW samples were found highly in accordance with that observed in the ZnMgO single layer within an error less than 1 meV, as shown in the figure, thus they could be regarded as the solid evidence supporting that the chemical compositions in the barrier layers are the same as that in the ZnMgO single-layer sample, because Raman shift is dependent on the Mg content in ZnMgO alloy [22]. As a consequence, we have a conclusion that the alloying effect between the barrier and the well layers is negligible, and the MQWs with well-defined multilayer structure have been fabricated in this study. The multiple-phonon RRS of the MQW samples were enhanced by ~2 orders of magnitude or even more in comparison with the ZnO epilayer, in which RRS was hardly observed in the PL spectrum. Using UV Raman spectroscopy, the LO phonon energy was accurately determined to be 75.9 ± 0.2 meV, ~3.9 meV higher than that of ZnO (72.0 ± 0.1 meV), thus the Mg content in the barrier layer was estimated to be ~15%, following Kong et al.'s study of alloying effect in ZnMgO films [22].

The PL as well as the multiple-phonon RRS was investigated by varying the temperature from RT down to ~12 K and an example is shown in Fig. 3(a). The PL intensity was monotonically increasing with the decrease in temperature, and could be well fitted by the PL quenching equation [23],

$$I(T) = \frac{I_0}{1 + a\exp(-E_a/kT)} \quad (1)$$

where $I(T)$ and I_0 are the integral PL intensities at a given temperature T and 0 K, respectively, a is a fitting parameter related to the lifetime of excitons, and E_a denotes the activation energy. For the

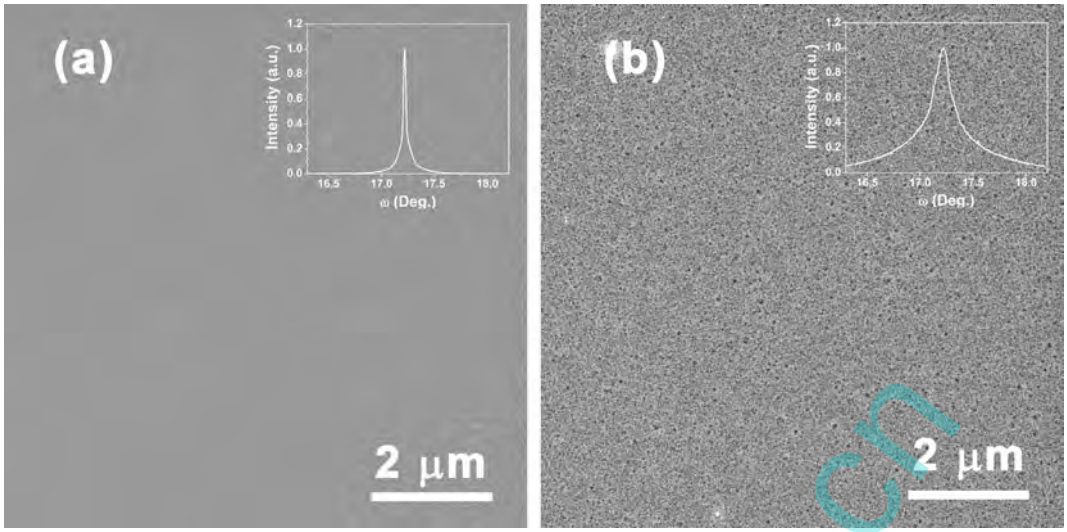

Fig. 1. SEM images of the ZnO (a) and ZnMgO (b) epilayers deposited at the optimized conditions of 800 °C and ~1 × 10^{-4} Pa. The insets are the corresponding rocking curves taken at (0002) diffraction of ZnO and ZnOMgO epilayers.

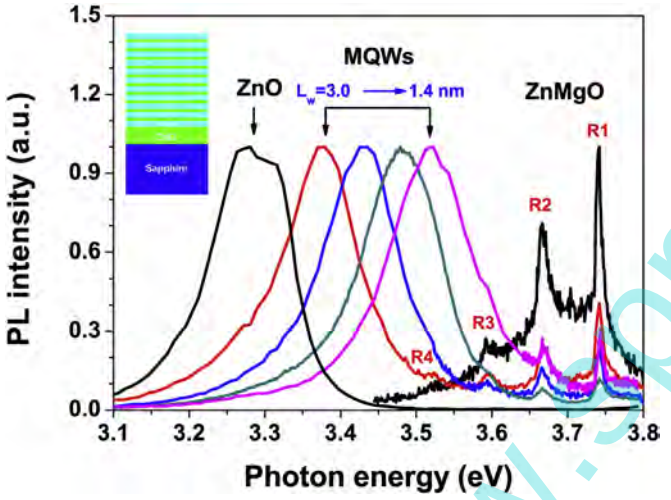

Fig. 2. PL spectra of the MQW samples taken at RT, in which the PL spectra of the ZnO and ZnMgO epilayers are included for comparison, and R1 to R4 indicates the first to the fourth order of the multiple-phonon RRS of incident light, respectively. The inset is the schematic diagram of the MQW samples with the thickness of well layers varying from 1.4 to 3 nm by maintaining the barrier layers at a constant thickness of ~7 nm.

MQW sample with 1.4-nm thick well layers, the fitted activation energy is $E_a = 27$ meV (Fig. S2), very close to the value reported by Makino et al. ($E_a = 28$ meV) [23]. With the decrease in temperature, the PL peak gradually shifted towards the high energy (Fig. S3), following the relationship of temperature-dependent band-gap energy by Ref. [4].

$$E_g(T) = E_g^0 - \frac{\alpha T^2}{T+\beta} \quad (2)$$

where E_g^0 is the band gap at 0 K, α and β are the temperature coefficients. At temperatures close to 12 K, the MQW samples exhibited a sharp PL peak with a width of ~40 meV, as shown in Fig. 3(b), which can be regarded as another evidence of the MQW samples having the well-defined and sharp interfaces between the barrier and the well layers, because the alloying effect and the interface width between the barrier and the well layers are the two major factors contributing to the broadening of PL peaks in MQW samples [24,25].

At a temperature below 100 K, the optical emission from the buffer layer started to be visible in the PL spectra, as indicated by D^0X (ZnO) in the figure, suggesting the MQW sample has a rather high quantum efficiency of radiative recombination in the well layers. In contrast with the PL from the buffer layer, the multiple-phonon Raman intensities maintain constant with the decrease in temperature, because Raman scattering is independent of the PL quantum efficiency and depends weakly on temperature, thus they looks weaker and weaker with rising PL background. Unlike some of reports in previous studies, no obvious PL except for the multiple-phonon RRS could be distinguished definitely from the barrier layers in the PL spectra from RT down to ~12 K, as shown in Fig. 3(a) and (b). Therefore, we further deduced that the excitons optically pumped in the barrier layers are high-efficiently transferred to the well layers before their radiative recombination.

Fig. 3(b) depicts the PL spectra of some MQW samples taken at ~12 K, in which PL spectra of the single-layer samples are included for comparison. The ZnO epilayer exhibits a sharp PL spectrum with a FWHM of ~7 meV, indicating the high quality of the sample, because this value is comparable with the PL peak measured from a single-crystal ZnO bulk material (~4 meV). As indicated in the figure, the bound exciton (D^0X) and the free exciton (FX) of ZnO are clearly distinguished at 3.365 and 3.378 eV, respectively. For the ZnMgO single-layer sample, the PL peak was shifted to 3.741 eV. We can see that the PL peak of the ZnMgO epilayer highly superimposes on the first order of Raman scattering of the incident light by LO phonons (R1), thus we deduce that the outgoing resonance is an important reason leading to the extreme enhancement in the first order of Raman scattering. Taking the Stokes shift between the absorption and emission into account, we believe that the ingoing and the outgoing resonance both contribute to the enhancement of the multiple-phonon RRS in this study. On the other hand, our "L" path for PL measurement might play an auxiliary role in detecting the multiple-phonon RRS because the Raman scattering by LO phonons in ZnO single crystal is much easier to detect in the setup of $x + z$ (yy) $x + z$ than in other ways [26]. For the ZnMgO single layer, the FWHM of PL peak was determined to be ~68 meV, being comparable with the samples grown on sapphire using radical source MBE [27]. There are two factors mainly contributing to the

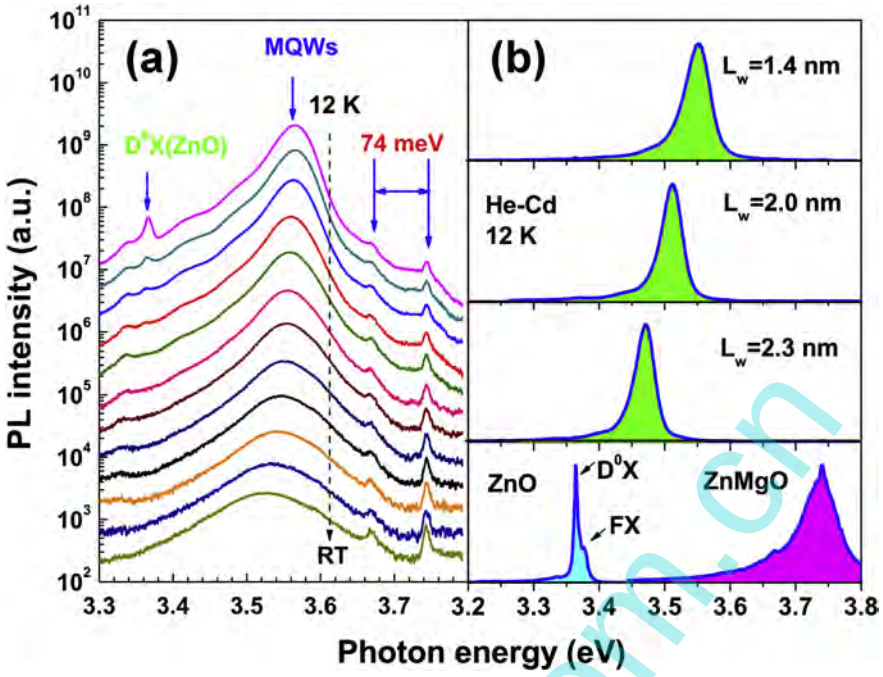

Fig. 3. (a) PL spectra of the MQW samples taken at the temperatures from RT to ~12 K, in which the PL peak indicated by D^0X (ZnO) is from the buffer layer. (b) PL spectra of the MQW samples with the given thickness of well layers taken at ~12 K, in which the PL spectra of the ZnO and ZnMgO epilayers are included for comparison.

PL broadening of ZnMgO alloys: (1) the configurations of the doped Mg atoms, which might lead to the band-gap broadening as large as 0.25 eV for $Zn_{0.75}Mg_{0.25}O$ alloy [28], and (2) the fluctuation in Mg concentration.

The band structure of ZnO/ZnMgO QW comes from a combination of the band gap and the offsets of the ZnMgO layer. For $Zn_{1-x}Mg_xO$ alloy, the band gap can be taken as $E_g^{ZnMgO} = E_g^{ZnO} + ax + bx^2$, where E_g^{ZnO} is the band gap of ZnO, a and b are the fitting parameters. The band gap of $Zn_{1-x}Mg_xO$ alloy was found linearly increasing with x up to 4.15 eV for $0 \le x \le 0.36$ in experiment [5,29], showing the bowing parameter b is 0 eV [4], but quite different a values were reported in literature. Using the commonly accepted values (a = 2.0–2.5), the Mg content in the $Zn_{1-x}Mg_xO$ film was estimated to be 0.15–0.19, in good agreement with our determination by multiple-phonon RRS. According to Makino et al. [16], the estimated Mg content is small enough for avoiding QCS and QCFK effects in the ZnO/ZnMgO MQW samples. On the other hand, the optical emission induced by QCS effect is invisible in the PL spectra of the MQW samples, thus the built-in internal electrical field was believed unimportant. Since the discontinuities at the conduction and valence bands (ΔE_c and ΔE_v) in ZnO/ZnMgO heterostructures have never been measured in a sufficient accuracy, we used $\Delta E_c/\Delta E_v = 9$ suggested by Ohtomo et al. [7], because this value was widely accepted in previous studies. If ZnO and ZnMgO have the same exciton binding energy ($E_b \approx 60$ meV), we have $\Delta E_c \approx 338$ meV and $\Delta E_v \approx 38$ meV.

Using the offsets, the PL energy shifts with respect to the PL peak of ZnO at ~12 K were calculated for the excitons confined in the MQWs with 7-nm-thick barrier layers, and then compared with the experimental data, as shown in Fig. 4, in which the inset schematically shows the offsets and the optical transition processes in the MQW samples. In our calculations, the exciton binding energy ($E_b \approx 60$ meV) was assumed independent of L_w. The PL shifts were calculated at the lowest energy states of excitons by graphically solving the solution equation of Kronig-Penney model [30]. We used $m_e^* = 0.28m_0$ (m_0 is the free-electron mass) as the effective

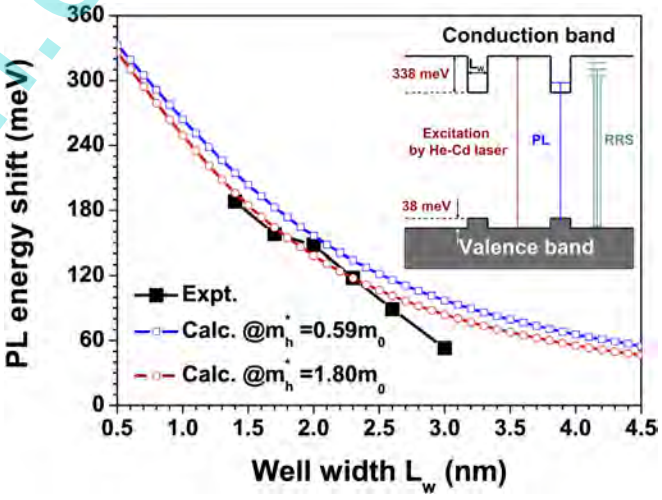

Fig. 4. PL energy shifts of the MQW samples with respect to the PL peak of ZnO at ~12 K. The theoretical results were calculated at the lowest energy states of excitons by solving the solution equation of Kronig-Penney model. The inset schematically shows the band offsets and the optical transition processes.

mass of an electron [7,8,31,32]. Two values, $m_h^* = 1.8m_0$ [7,8] and $m_h^* = 0.59m_0$ [31,32], which could be regarded as the upper and the lower limits, were used as the effective mass of a hole, respectively. As a matter of fact, the two holes with quite different effective masses lead to L_w-dependent PL shifts close to each other, as shown in the figure. At ~12 K, QC effects produced a blue-shift of the PL peak by 53–188 meV for the MQW samples with L_w = 3.0–1.4 nm, respectively, in good agreement with the calculated results using $m_h^* = 1.8m_0$. We noticed that the discrepancy between the calculated and experimental data is increased when $L_w \ge 2.6$ nm. Similar increase in the discrepancy could also be observed in Makino et al.'s report on the optical properties of $[ZnO/Zn_{0.85}Mg_{0.15}O]_{10}$ MQWs

grown on sapphire substrate [8]. Though the inhomogeneity of the MQW samples could produce uncertainty in determining the PL energy, we would like to ascribe the increase in the discrepancy to the decrease in crystallinity, because the ascription is supported by our RSM measurement. If the internal electric field is supposed to be responsible for the discrepancy between the calculated and experimental results, the built-in internal electric field is estimated to be ~0.05 and ~0.1 MV/cm for the MQW samples with $L_w = 2.6$ and 3.0 nm, respectively, which are at a rather low level for ZnO/ZnMgO MQWs.

4. Conclusions

In conclusion, ZnO/ZnMgO MQW samples were fabricated using PLD method at the optimized conditions of 1×10^{-4} Pa and 800 °C. No obvious QCS effect was observed, while extremely enhanced multiple-phonon RRS appeared in the PL spectra when the MQW samples were excited by a 325-nm He-Cd laser. The multiple-phonon RRS are highly in accordance with that observed in the ZnMgO epilayer, thus being the solid evidence that the MQW samples have well-defined multilayer structure, and the alloying effect between the barrier and the well layers is negligible. Using the multiple-phonon RRS as well as the PL peak energy of ZnMgO epilayer, the Mg content in the barrier layers was estimated to be 0.15–0.19, providing the offsets of $\Delta E_c \approx 338$ meV and $\Delta E_v \approx 38$ meV. At low temperature of ~12 K, QC effect produced a blue-shift of the PL peak by 53–188 meV for the MQW samples with $L_w = 3.0$–1.4 nm, quantitatively in good agreement with the calculated results using the Kronig-Penney model with $m_h^* = 1.8m_0$.

Acknowledgement

The research is supported by the National Natural Science Foundation of China under Grant No. 10774018 and Basic Research Project for Key Laboratory of Liaoning Province under Grant No. LZ2014006. One of authors, J. M. Ashfaq, would like to thank the support of Chinese Government Scholarship (2011GXZR70).

Appendix A. Supplementary data

Supplementary data related to this article can be found at http://dx.doi.org/10.1016/j.jallcom.2016.04.150.

References

[1] P. Yu, Z.K. Tang, G.K.L. Wong, M. Kawasaki, A. Ohtomo, H. Koinuma, Y. Segawa, Solid State Commun. 103 (1997) 459.
[2] Z.K. Tang, G.K.L. Wong, P. Yu, M. Kawasaki, A. Ohtomo, H. Koinuma, Y. Segawa, Appl. Phys. Lett. 72 (1998) 3270.
[3] D.M. Bagnall, Y.F. Chen, Z. Zhu, T. Yao, S. Koyama, M.Y. Shen, T. Goto, Appl. Phys. Lett. 70 (1997) 2230.
[4] Ü. Özgür, Ya. I. Alivov, C. Liu, A. Teke, M.A. Reshchikov, S. Doğan, V. Avrutin, S.-J. Cho, H. Morkoç, J. Appl. Phys. 98 (041301) (2005).
[5] A. Ohtomo, M. Kawasaki, T. Koida, K. Masubuchi, H. Koinuma, Y. Sakurai, Y. Yoshida, T. Yasuda, Y. Segawa, Appl. Phys. Lett. 72 (1998) 2466.
[6] A. Ohtomo, K. Tamura, M. Kawasaki, T. Makino, Y. Segawa, Z.K. Tang, G.K.L. Wong, Y. Matsumoto, H. Koinumac, Appl. Phys. Lett. 77 (2000) 2204.
[7] A. Ohtomo, M. Kawasaki, I. Ohkubo, H. Koinuma, T. Yasuda, Y. Segawa, Appl. Phys. Lett. 75 (1999) 980.
[8] T. Makino, C.H. Chia, N.T. Tuan, H.D. Sun, Y. Segawa, M. Kawasaki, A. Ohtomo, K. Tamura, H. Koinuma, Appl. Phys. Lett. 77 (2000) 975.
[9] S. Sadofev, S. Blumstengel, J. Cui, J. Puls, S. Rogaschewski, P. Schäfer, Y.G. Sadofyev, F. Henneberger, Appl. Phys. Lett. 87 (091903) (2005).
[10] C.W. Sun, P. Xin, Z.W. Liu, Q.Y. Zhang, Appl. Phys. Lett. 88 (2006) 221914.
[11] X.Q. Gu, L.P. Zhu, Z.Z. Ye, H.P. He, Y.Z. Zhang, F. Huang, M.X. Qiu, Y.J. Zeng, F. Liu, W. Jaeger, Appl. Phys. Lett. 91 (022103) (2007).
[12] J.-M. Chauveau, M. Teisseire, H. Kim-Chauveau, C. Deparis, C. Morhain, B. Vinter, Appl. Phys. Lett. 97 (081903) (2010).
[13] J.W. Sun, Y.M. Lu, Y.C. Liu, D.Z. Shen, Z.Z. Zhang, B.H. Li, J.Y. Zhang, B. Yao, D.X. Zhao, X.W. Fan, J. Phys. D Appl. Phys. 40 (2007) 6541.
[14] H.C. Wang, C.-H. Liao, Y.-L. Chueh, C.-C. Lai, L.-H. Chen, R.C.-C. Tsiang, Opt. Mater. Express 3 (2013) 237.
[15] Y.-S. Choi, J.-W. Kang, B.-H. Kim, S.-J. Park, Opt. Express 21 (2013) 31560.
[16] T. Makino, K. Tamura, C.H. Chia, Y. Segawa, M. Kawasaki, A. Ohtomo, H. Koinuma, Appl. Phys. Lett. 81 (2002) 2355.
[17] C. Morhain, T. Bretagnon, P. Lefebvre, X. Tang, P. Valvin, T. Guillet, B. Gil, T. Taliercio, M. Teisseire-Doninelli, B. Vinter, C. Deparis, Phys. Rev. B 72 (2005) 241305R.
[18] B.P. Zhang, B.L. Liu, J.Z. Yu, Q.M. Wang, C.Y. Liu, Y.C. Liu, Y. Segawa, Appl. Phys. Lett. 90 (2007) 132113.
[19] M. Brandt, M. Lange, M. Stölzel, A. Müller, G. Benndorf, J. Zippel, J. Lenzner, M. Lorenz, M. Grundmann, Appl. Phys. Lett. 97 (052101) (2010).
[20] J.M. Ashfaq, B.C. Hu, N. Zhu, X.L. Li, C.Y. Ma, Q.Y. Zhang, J. Lumin. 158 (2015) 211.
[21] A. Ohtomo, A. Tsukazaki, Semicond. Sci. Technol. 20 (2005) S1.
[22] J.F. Kong, W.Z. Shen, Y.W. Zhang, C. Yang, X.M. Li, Appl. Phys. Lett. 92 (2008) 191910.
[23] T. Makino, K. Tamura, C.H. Chia, Y. Segawa, M. Kawasaki, A. Ohtomo, H. Koinuma, J. Appl. Phys. 93 (2003) 5929.
[24] G. Coli, K.K. Bajaj, J. Li, J.Y. Lin, H.X. Jiang, Appl. Phys. Lett. 80 (2002) 2907.
[25] J. Singh, K.K. Bajaj, J. Appl. Phys. 57 (1985) 5433.
[26] T.C. Damen, S.P.S. Porto, B. Tell, Phys. Rev. 142 (1966) 570.
[27] H. Shibata, H. Tampo, K. Matsubara, A. Yamada, K. Sakurai, S. Ishizuka, S. Niki, M. Sakai, Appl. Phys. Lett. 90 (2007) 124104.
[28] C.Y. Pu, D.W. Zhou, Z. Wang, Q.Y. Zhang, C.P. Li, Sci. Sin. Phys. Mech. Astron. 43 (2013) 941.
[29] I. Takeuchi, W. Yang, K.-S. Chang, M.A. Aronova, T. Venkatesan, R.D. Vispute, L.A. Bendersky, J. Appl. Phys. 94 (2003) 7336.
[30] C. Kittel, Introduction to Solid State Physics, fifth ed., John Wiley & Sons, New York, 1976, p. 192.
[31] B.K. Meyer, H. Alves, D.M. Hofmann, W. Kriegsies, D. Forster, F. Bertram, J. Christen, A. Hofmann, M. Straβburg, M. Dworzak, U. Haboeck, A.V. Rodina, Phys. Stat. Sol. (b) 241 (2004) 231.
[32] Th. Gruber, C. Kirchner, R. Kling, F. Reuss, A. Waag, Appl. Phys. Lett. 84 (2004) 5359.